metals

MDPI

Article

Improving Maraging Steel 350 Machinability via Wiper Insert-Enhanced Face Milling

Adel T. Abbas [1,*], Mohamed O. Helmy [2,*], Khalid F. Alqosaibi [1], Shahid Parvez [1], Ali S. Hasan [1] and Ahmed Elkaseer [3]

[1] Department of Mechanical Engineering, College of Engineering, King Saud University, P.O. Box 800, Riyadh 11421, Saudi Arabia; kalqosaibi@ksu.edu.sa (K.F.A.); sparvez@ksu.edu.sa (S.P.)
[2] Department of Mechanical Engineering, Benha Faculty of Engineering, Benha University, Benha 13518, Egypt
[3] Institute for Automation and Applied Informatics, Karlsruhe Institute of Technology, 76344 Eggenstein-Leopoldshafen, Germany; ahmed.elkaseer@kit.edu
* Correspondence: aabbas@ksu.edu.sa (A.T.A.); mohamed.osama@bhit.bu.edu.eg (M.O.H.)

Abstract: Despite the prevalent application of 18% Ni maraging steel in critical sectors such as aerospace and automotive due to its unique characteristics, including high ductility, yield strength, and hardenability, its machining presents enormous challenges, categorizing it as a difficult-to-machine material. The cutting tool's geometry is crucial in machining, significantly affecting chip formation, cutting forces, power consumption, and obtainable surface quality. In particular, wiper insert technology, characterized by its multi-radius design, offers an increased contact area compared to conventional inserts, potentially enhancing the quality of the machined surface. This study explores the effectiveness of wiper inserts in the face-milling of maraging steel 350, conducting a comparative analysis across three distinct machining setups. These setups vary by alternating the number of wiper and conventional inserts within the same cutter, thereby examining the influence of insert configuration on machining outcomes. The research employs a reliable and well-established statistical approach to evaluate how different variables, such as cutting speed and feed rate, affect surface quality, power consumption, and material removal rate (MRR). It also sheds light on the material removal mechanisms facilitated by each type of insert. The findings reveal that incorporating a higher number of wiper inserts significantly enhances the surface finish but concurrently increases power consumption. Thus, the study successfully identifies an optimal set of process parameters that attain a balance between achieving superior surface quality and maintaining energy efficiency in the machining of maraging steel 350. This balance is crucial for optimizing manufacturing processes while adhering to the stringent quality and sustainability standards required in aerospace and automotive manufacturing.

Keywords: maraging steel; wiper insert; surface quality; power consumption; productivity; grey relational analysis

Citation: Abbas, A.T.; Helmy, M.O.; Alqosaibi, K.F.; Parvez, S.; Hasan, A.S.; Elkaseer, A. Improving Maraging Steel 350 Machinability via Wiper Insert-Enhanced Face Milling. *Metals* **2024**, *14*, 514. https://doi.org/10.3390/met14050514

Academic Editor: Jorge Salguero

Received: 13 March 2024
Revised: 21 April 2024
Accepted: 25 April 2024
Published: 28 April 2024

1. Introduction

Maraging steel, an alloy known for its exceptional strength and toughness, derives its name from a unique two-step process: 'martensite' transformation followed by 'aging'. Initially, the steel exhibits a martensitic phase that is particularly hard and brittle. Then, the aging treatment of steel is shifted to an aging treatment to refine this brittleness and improve its suite of mechanical properties. This treatment entails heating the steel to a relatively moderate temperature range, specifically between 500 °C and 600 °C, for a predetermined duration, which in turn precipitates intermetallic compounds that substantially increase the steel's strength while maintaining its ductility [1,2]. The resultant advanced material boasts properties that are in high demand for critical engineering applications, including but not limited to aerospace components, landing gear, helicopter undercarriages,

rocket motors, and missile casings. The unique characteristics of maraging steels, such as their exceptional strength, wear resistance, and high-pressure resilience, make them ideal for specific industrial uses such as injection molds and dies [3,4]. Through precise control over the aging parameters, including temperature and duration, it is possible to engineer ultra-high-strength maraging steels tailored for sophisticated aerospace and nuclear applications [5]. The necessity for superior machined surface quality in these steels cannot be overstated, given its profound impact on industrial adherence standards, which influences the components' fatigue life, corrosion resistance, and dimensional stability [6]. Nonetheless, the process of machining these high-performance materials is fraught with challenges. The remarkable properties of the maraging steel result in high cutting forces during machining, which increase the required cutting energy and cutting temperature, reduce surface quality, and ultimately diminish the tool's lifespan [7].

Achieving high-precision machined parts typically involves a sequence of roughing and finishing operations. However, an alternative strategy suggests integrating these stages into a single, optimized process. In this context, the primary cutting variables, including cutting speed, feed rate, and depth of cut, play critical roles in determining both the tool's endurance and the surface quality of parts. Specifically, research has highlighted the significant interplay between cutting speed and feed rate, especially regarding their impact on the surface finish of maraging steel 350 [2]. In contrast, studies on SAE 8620 and EN9 tool steels revealed that feed rate is the paramount factor influencing surface quality [8]. Further investigation by D'addona, D. M., and Sunil J. Raykar corroborated the dominance of feed rate in surface quality outcomes, with depth of cut and insert type also being influential factors [9]. Therefore, the meticulous optimization of these parameters is vital for improving the surface finish. To this end, several advanced methodologies, such as artificial neural networks (ANN), grey relational analysis (GRA), fuzzy logic, and response surface methodology (RSM), have been effectively employed to fine-tune machining conditions [10].

In specific machining contexts, the tool's geometry can restrict the adjustability of process parameters necessary for achieving the desired surface quality in line with industrial benchmarks [11]. While multi-coated tools have been developed to increase cutting speeds and thereby lessen cutting forces [12,13], cubic boron nitride (CBN) tools stand out for their superior performance, especially at elevated cutting speeds compared to their coated carbide counterparts. CBN tools exhibit remarkable wear resistance even under high-speed machining conditions for tool steel materials. This exceptional durability not only extends the tool's lifespan but also has a profound influence on the residual stresses and surface quality of the machined parts [14,15]. However, adjusting the nose radius of CBN inserts has been found to enhance the surface quality of AISI D2 steel, whereas an increase in feed rate tends to degrade it [16]. Furthermore, a study by Yang and Zhanqiang on the impact of varying turning parameters on Inconel 718's surface quality revealed that cutting speed had a negligible impact on the surface finish. In contrast, the feed rate and the tool's nose radius emerged as the critical factors determining surface finish [17,18].

In the pursuit of enhancing tool performance, significant advancements have been made in tool geometry. In particular, the introduction of wiper inserts, which feature multi-radius geometry, allows for higher feed rates while maintaining surface quality [19]. These inserts reduce cutting pressure, leading to improvements in machined surface quality and a reduction in vibrations when compared to traditional single-nose radius inserts [20,21]. For instance, tests with oil-hardened non-shrinking steel (OHNS) demonstrated that using a wiper insert produced better surface finishes than conventional inserts with standard nose radii [9]. Beyond their efficacy in chip control at low feed rates, wiper inserts also facilitate smooth chip breaking at higher feed rates and offer a larger contact area than conventional inserts, enhancing surface finishes at increased feed rates [22,23]. Zhang et al. found that wiper inserts surpassed conventional inserts in material removal rate (MRR) and surface quality when turning AISI 1045 steel [24]. In a similar vein, Davim et al. determined that wiper tools are superior for achieving high surface quality and extending

tool life, although conventional tools have the benefit of lower cutting forces and power consumption [25]. Additionally, Elbah et al. discovered that ceramic wiper inserts could improve the surface quality of hardened AISI 4140 steel 2.5-fold compared to traditional inserts [26]. Comparisons during the turning of Monel K500 in dry and minimal quality lubrication conditions also demonstrated a substantial 73.86% improvement in surface quality with wiper inserts over conventional nose radius inserts [27].

Moreover, wiper inserts significantly reduce cutting forces by 57% at elevated feed rates due to the thinner uncut chip thickness characteristic of these inserts, which helps in lowering cutting forces, cutting temperatures, and surface roughness [27,28]. Remarkably, wiper inserts can achieve the same level of surface quality at twice the feed rate compared to what is achievable with conventional inserts [2,29]. This means that wiper inserts are capable of maintaining equivalent surface quality at a feed rate that is double that of conventional inserts, an outcome unattainable by the latter under similar conditions [23,30,31]. In other words, under certain machining parameters, wiper inserts can achieve a surface quality comparable to that of grinding operations [32–34]. When a wiper insert coated with carbide is used in cutting stainless steel, it reduces the peak-to-valley surface roughness and enhances the material removal rate (MRR) [35]. A wiper insert can achieve an arithmetic average roughness of less than 0.5 μm in turning of AISI D2 steel, which is a significant improvement over the 0.8 μm roughness level obtained with conventional inserts [25,36].

The conducted review of existing literature highlights the enhanced productivity and superior surface quality afforded by wiper inserts in machining operations. Despite these benefits, conventional tools remain the prevalent choice for machining maraging steel 350, highlighting a significant gap in research and application regarding advanced tool technologies for this material. This gap emphasizes the urgency of exploring the capabilities of wiper inserts with different configurations in the face-milling of maraging steel 350, a material known for its exceptional properties and demanding application requirements.

In this study, we probe into the performance of wiper inserts in face-milling maraging steel 350 by implementing three distinct machining scenarios. These scenarios were methodically designed by varying the configuration of the wiper and standard inserts within the same milling cutter, providing a nuanced understanding of how wiper edge length influences key outcomes, including surface quality, MRR, and power consumption. Each scenario was rigorously tested across six feed rate levels and two cutting speed levels to ensure a comprehensive evaluation under varied conditions. Additionally, the interaction between the tool and workpiece was meticulously analyzed for both wiper and standard inserts to uncover detailed insights into their operational efficacy. To further refine the process, an optimization study using GRA was conducted. This optimization aimed to determine the most effective combination of process parameters, balancing the goals of maximizing productivity and surface quality while minimizing power consumption. By addressing this research gap, the study aims to provide a robust framework for understanding the potential of wiper inserts in enhancing the machining efficiency of maraging steel 350, paving the way for more informed tool selection and process optimization in industrial applications.

2. Material and Methodology

This study utilizes maraging steel 350, provided in the form of a 32 mm-thick plate via hot-rolling and subsequent air-cooling to achieve its desired mechanical properties and microstructure. To precisely characterize the steel's composition, a cutting-edge Spectro Graphical Analyzer, the SPECTROMAXx—LMM05 model from AMETEK Inc., based in Berwyn, PA, USA, is employed. The analyzer provides an accurate quantification of the steel's chemical constituents, the details of which are methodically cataloged in Table 1.

Table 1. Weight percentage chemical composition for maraging steel 350.

Element	Ni	Co	Mo	Ti	Al	Cu	C	Cr	Mn	Fe
weight %	18.164	12.173	4.06	2.211	0.147	0.010	0.032	0.004	0.022	Remaining Balance

The chemical composition of such material is crucial, as it directly influences the alloy's mechanical properties, machinability, and response to heat treatment and aging processes. The linkage between chemical composition and material properties has been substantiated by the foundational research of Abbas et al. [2], who meticulously examined the microstructures of similar materials. Their work offers valuable insights into the intrinsic characteristics that govern the behavior of maraging steel 350 during machining and post-processing.

The tensile properties of such material were evaluated using an INSTRON-5984 Universal Testing Machine, supplied by Instron Corporation, located in Norwood, MA, USA. This examination was conducted on a 34-mm tensile round bar specimen with a diameter of 6.2 mm to ascertain the material's mechanical characteristics under tension. The crosshead speed was maintained at 2 mm/min during the testing, equating to an initial strain rate of 1×10^{-3} per second. The outcomes of these tensile tests, which provide crucial insights into the steel's strength and ductility, are systematically presented in Table 2.

Table 2. Tensile properties for maraging steel 350.

Property	Test Value
Ultimate tensile strength, MPa	1132
Yield strength, MPa	1080
Young's modulus, GPa	200
Elongation %	22.5
Hardness, HRc	38

The workpieces utilized in the face-milling experiments are rectangular cuboids with $100 \times 50 \times 30$ mm dimensions for length, width, and height, respectively. These experiments were conducted on a vertical milling machine, specifically the Emco C40, manufactured by Emco in Salzburg, Austria. This machine features a spindle with a power capacity of 13 KW and can operate at variable speeds ranging from 10 to 5000 RPM. Additionally, it offers a feed rate that varies from 10 to 2000 mm/min.

A cutter from Sandvik, based in Stockholm, Sweden, was employed for the face-milling operations. This cutter, designated as R245-063Q22-12M, is designed to hold five inserts. The experimental setup was varied across three different scenarios to investigate the impact of insert configuration on the milling process:

Setup 1 utilizes five conventional inserts.

Setup 2 combines four conventional inserts with one wiper insert.

Setup 3 employs three conventional inserts alongside two wiper inserts.

These configurations are visually depicted in Figure 1, illustrating the arrangement of the wiper and standard inserts. The conventional inserts are identified by the code R245-12T3M-PM and feature four cutting edges with a PVD AlTiCrN coating, as detailed in Figure 2a. On the other hand, the wiper inserts, specified by the code R245-12 T3 E-W, have a single cutting edge and are coated with PVD TiAlN, which is demonstrated in Figure 2b. The detailed specifications for both the wiper and standard inserts are systematically cataloged in Table 3, providing a comprehensive overview for further analysis and discussion of the experiment results.

(**a**) (**b**) (**c**)

Figure 1. The three sets of insert setup. (**a**) First setup with (5) conventional inserts, (**b**) second setup with (4) conventional inserts and (1) wiper insert, (**c**) third setup with (3) conventional inserts and (2) wiper inserts.

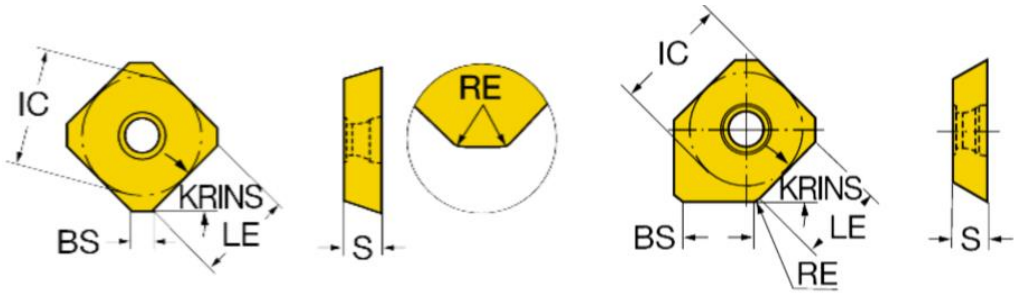

(**a**) (**b**)

Figure 2. Geometry details of (**a**) standard insert and (**b**) wiper insert, Reprinted with permission from ref. [22]. 2024 AB Sandvik Coromant.

Table 3. Specifications of standard and wiper inserts.

Parameters	Units	Insert Type	
		Conventional	Wiper
Inscribed circle diameter (IC)	mm	13.4	
Corner radius (RE)	mm	1.5	
Cutting edge effective length (LE)	mm	10	
Major cutting-edge angle (KRINS)	deg	45	
Insert thickness (S)	mm	4	
Wiper edge length (BS)	mm	2	8.2

The overall design of the test process consists of 36 experiments, with 12 experiments dedicated to each setup. The test is conducted at two speed levels, 30 and 60 m/min, with a fixed depth of 0.5 mm. The feed per tooth is set at multiple levels, starting from 0.04 mm with an increment of 0.02 mm/tooth up to a maximum of 0.14 mm, resulting in six distinct levels. Conversely, the length of the cut is fixed at 100 mm, and the width of the cut is fixed at 50 mm for all experiments. The tests are conducted in flood coolant conditions. Each test is performed twice, and the average of the two readings is used for evaluation purposes to enhance statistical accuracy. All cutting conditions were defined after consultation with a tool manufacturing expert (Sandvik Expert). The test rig for machining samples is depicted in Figure 3.

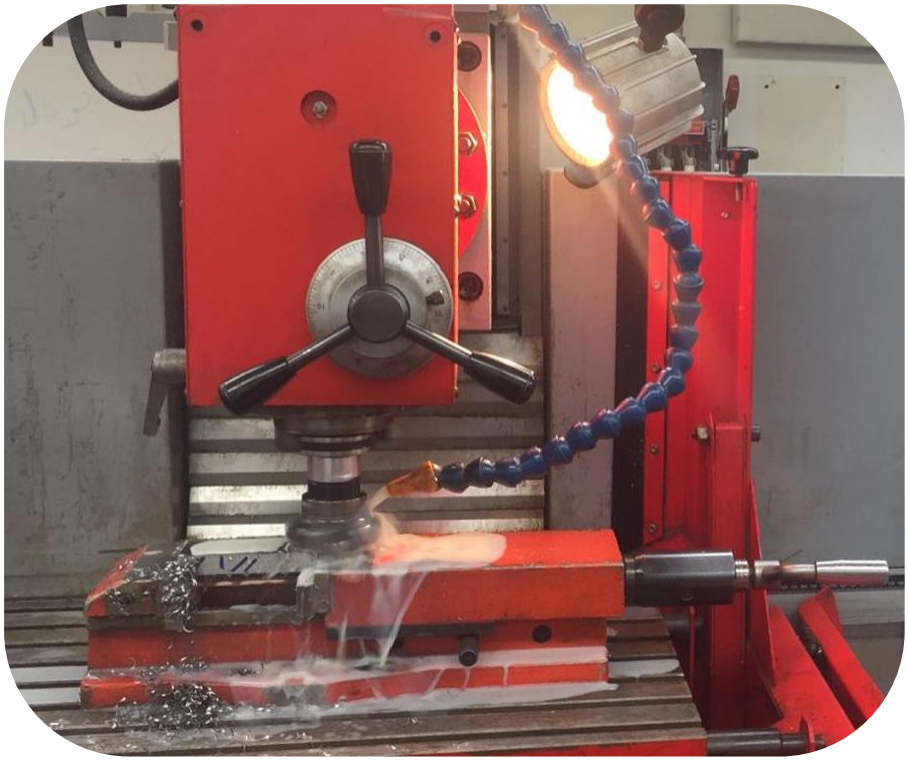

Figure 3. Experimental setup of face-milling of maraging at flood coolant condition.

A standard surface roughness tester, Tesa-Rougossurf-90G from the Tesa company in Bugnon, Switzerland, was utilized for measuring surface roughness, as illustrated in Figure 4. The surface roughness parameters, arithmetic average roughness (Ra), total height of the roughness profile (Rt), and maximum height of the roughness profile (Rz) were measured in the same feed direction to capture the topography of the machined surface. The settings for measuring surface roughness were as follows: cut-off length: 0.8 mm; measurement surface: plain; measurement speed: 1 mm/s; cut-off number: 19; gauge type: skid.

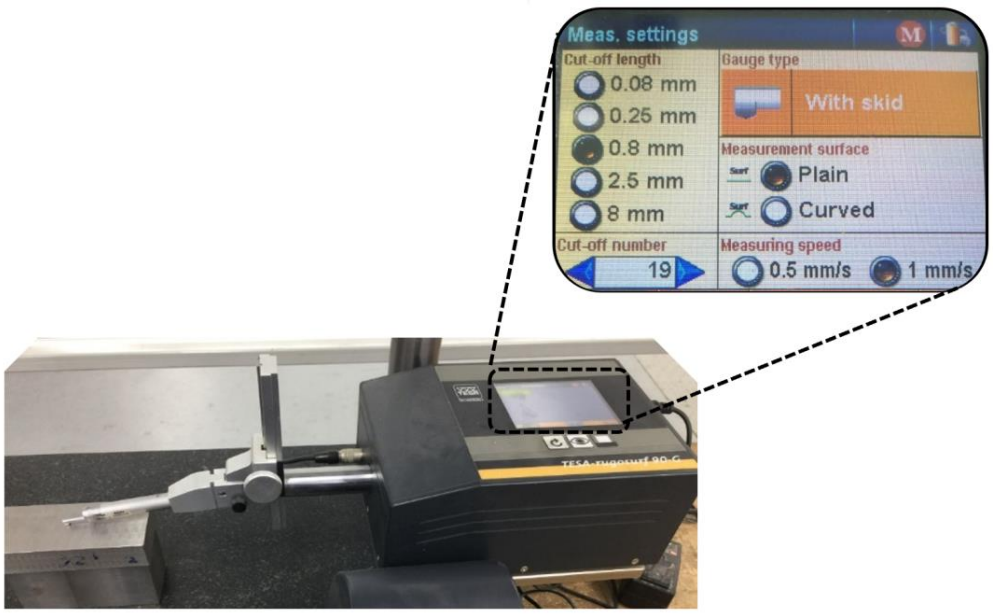

Figure 4. Parameters of surface roughness tester.

Power consumption in machining was monitored using two power meters (Tactix 403057, Beijing, China). These meters were connected to the power supply of the milling machine to monitor the voltage and current during the machining process. Power consumption was assessed by measuring the current (I) in one line and the voltage potential (V) across a balanced three-phase load of the milling machine. The configuration for power measurement is depicted in Figure 5. For each milling run, voltage and current were recorded in three sets, with the average being calculated for power assessment. The power (P) is determined using the voltage, current, and power factor (ø) for a three-phase machine as follows:

$$P = V \times I \times \sqrt{3} \times \cos \varnothing \quad (1)$$

where current is in amperes, voltage is in volts, and power is in watts.

Figure 5. Test rig for power consumption measurement.

3. Tool–Workpiece Engagement

The surface topography resulting from the interference between the tool and workpiece is indicative of the machined surface quality. In this context, Chen et al. have devised a 'maximum height method' to predict the surface profile using the milling cutter's end edges [37]. This technique allows for the transformation of the end edges of both wiper and standard inserts into planar curves, as depicted in Figure 6. The paths traced by these edges along the tool path for the three different configurations of the wiper and standard inserts are illustrated in Figure 7a, Figure 7b, and Figure 7c, respectively.

The multi-radius technology of the wiper insert significantly diminishes the feed line peaks owing to its larger contact area with the workpiece compared to a standard insert, thereby improving surface quality. In particular, the third configuration, which incorporates two wiper inserts, achieves a superior surface finish compared to the other scenarios, as demonstrated in Figure 7c. This outcome highlights the effectiveness of wiper inserts in enhancing the surface finish in milling operations.

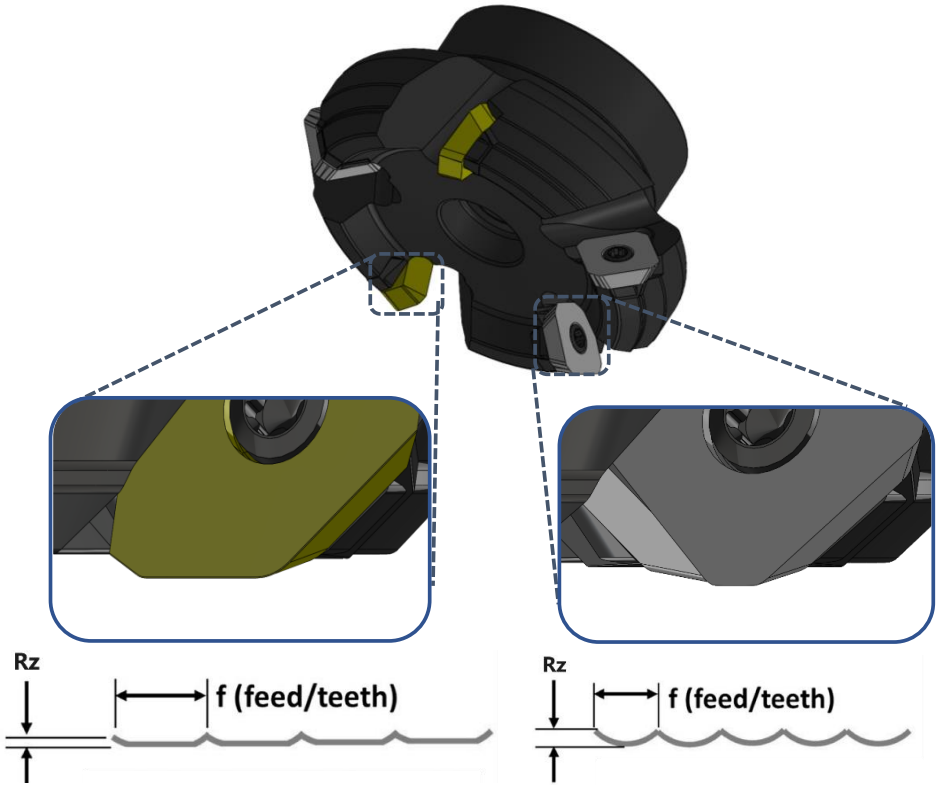

(**a**) Wiper insert with wiper length (BS) of 8.2 mm

(**b**) Standard insert with wiper length (BS) of 2 mm

Figure 6. Surface topography obtained by (**a**) wiper and (**b**) standard insert.

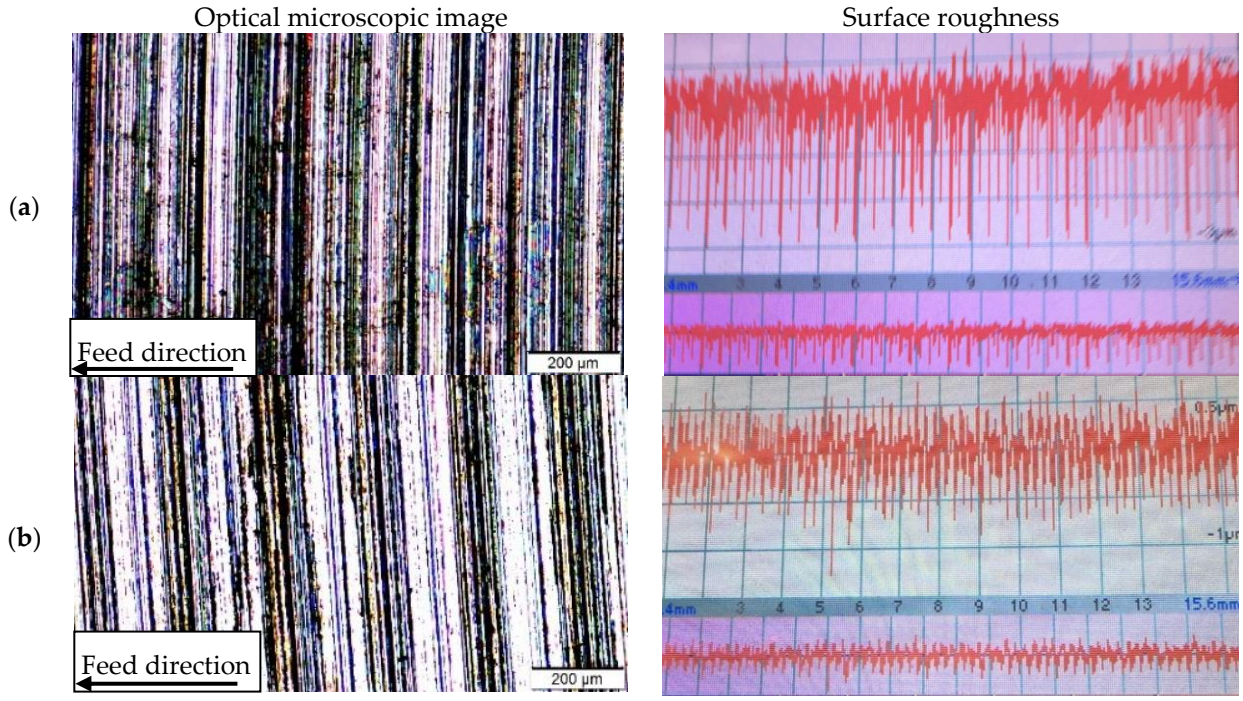

Figure 7. *Cont.*

(**c**)

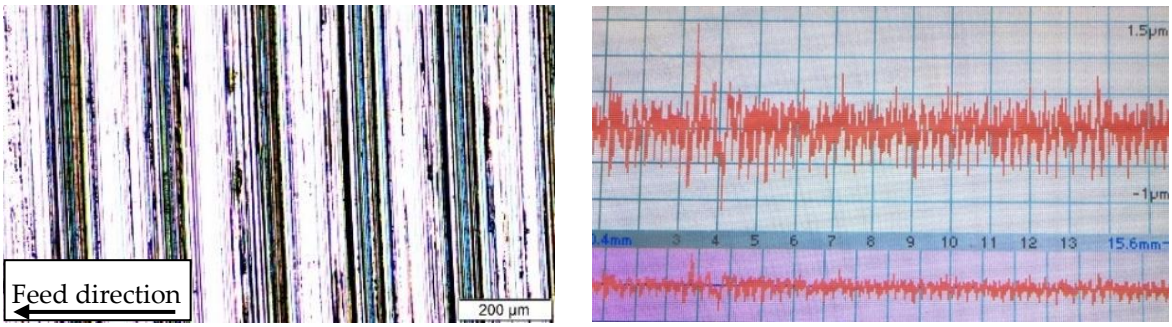

Figure 7. Optical microscopic and surface roughness tester images for the same cutting conditions: surface speed = 60 m/min, feed rate 0.04 mm/tooth, and depth of 0.5 mm (**a**) Experiment # 7 represents the first setup, (**b**) Experiment # 19 represents the second setup, and (**c**) Experiment # 31 represent the third setup.

4. Results and Discussion

The impact of varying the number of wiper inserts is systematically assessed across six different feed rate levels and two distinct cutting speed levels while maintaining a constant depth of cut, detailed in Table 4. This evaluation examines their influence on several critical responses, specifically surface roughness, PC, and MRR. The investigation is structured to analyze how these key performance indicators respond to the adjustments in the number of wiper inserts under the given machining conditions, providing insights into the optimal use of wiper inserts in milling operations to achieve desired efficiency and surface quality outcomes.

Table 4. Experiment plan for machining maraging steel 350 with their results.

Test No.	Type of Setup	Speed m/min	Feed Rate (mm/tooth)	Surface Roughness, µm			Power Consumption (KW)	MRR (mm^3/min)
				Ra	Rt	Rz		
1	First scenario (5 Conventional Inserts)	30	0.04	0.591	4.341	3.969	1.167	760
2		30	0.06	0.643	4.207	3.812	1.187	1140
3		30	0.08	0.657	3.829	3.193	1.207	1520
4		30	0.10	0.757	4.736	4.017	1.220	1900
5		30	0.12	0.805	4.004	3.527	1.234	2280
6		30	0.14	0.859	6.113	5.070	1.254	2660
7		60	0.04	0.486	2.995	2.655	1.447	1515
8		60	0.06	0.518	3.925	3.413	1.500	2273
9		60	0.08	0.549	2.977	2.731	1.567	3030
10		60	0.10	0.563	5.452	3.726	1.607	3788
11		60	0.12	0.643	4.588	3.836	1.660	4545
12		60	0.14	0.731	5.031	4.180	1.707	5303

Table 4. *Cont.*

Test No.	Type of Setup	Speed m/min	Feed Rate (mm/tooth)	Surface Roughness, µm			Power Consumption (KW)	MRR (mm^3/min)
				Ra	Rt	Rz		
13	Second scenario (4 Conventional + 1 Wiper Insert)	30	0.04	0.384	2.822	2.580	1.214	760
14		30	0.06	0.418	2.735	2.478	1.234	1140
15		30	0.08	0.427	2.489	2.075	1.254	1520
16		30	0.10	0.492	3.078	2.611	1.267	1900
17		30	0.12	0.523	2.603	2.293	1.280	2280
18		30	0.14	0.558	3.973	3.296	1.307	2660
19		60	0.04	0.316	1.947	1.726	1.507	1515
20		60	0.06	0.337	2.551	2.218	1.560	2273
21		60	0.08	0.357	1.935	1.775	1.627	3030
22		60	0.10	0.366	3.544	2.422	1.674	3788
23		60	0.12	0.418	2.982	2.493	1.727	4545
24		60	0.14	0.475	3.270	2.717	1.774	5303
25	Third scenario (3 Conventional + 2 Wiper Inserts)	30	0.04	0.278	2.040	1.865	1.247	760
26		30	0.06	0.302	1.977	1.792	1.274	1140
27		30	0.08	0.309	1.800	1.501	1.294	1520
28		30	0.10	0.356	2.226	1.888	1.307	1900
29		30	0.12	0.378	1.882	1.658	1.320	2280
30		30	0.14	0.404	2.873	2.383	1.340	2660
31		60	0.04	0.228	1.408	1.248	1.547	1515
32		60	0.06	0.243	1.845	1.604	1.607	2273
33		60	0.08	0.258	1.399	1.284	1.680	3030
34		60	0.10	0.265	2.562	1.751	1.720	3788
35		60	0.12	0.302	2.156	1.803	1.780	4545
36		60	0.14	0.344	2.365	1.965	1.827	5303

4.1. Effect of Process Parameters on Surface Roughness

Figure 8 illustrates the impact of feed rate on Ra at two cutting speed levels, 30 m/min and 60 m/min, across three machining scenarios: one with five conventional inserts, another with four conventional inserts plus one wiper insert, and the last featuring three conventional inserts with two wiper inserts. It is revealed that Ra escalates with an increase in feed rate across all scenarios, attributed to the augmented chip thickness, which amplifies the surface waviness. Conversely, a higher cutting speed tends to decrease the uncut chip thickness, resulting in smoother surfaces.

The inclusion of wiper inserts remarkably reduces the Ra values compared to scenarios utilizing only standard inserts. This improvement is owed to the larger contact area provided by the wiper insert when engaged with the workpiece, as detailed in Section 3. Integrating two wiper inserts within the cutter can further enhance this effect by increasing the likelihood of overlap between the wiper inserts, thereby extending the wiper edge length and refining the machined surface quality. Nevertheless, it is important to note that wiper inserts are typically more costly than standard ones. Hence, there is a critical need to optimize the number of wiper inserts and adjust the process parameters wisely to balance achieving high productivity and superior surface finish while maintaining cost-efficiency in machining operations.

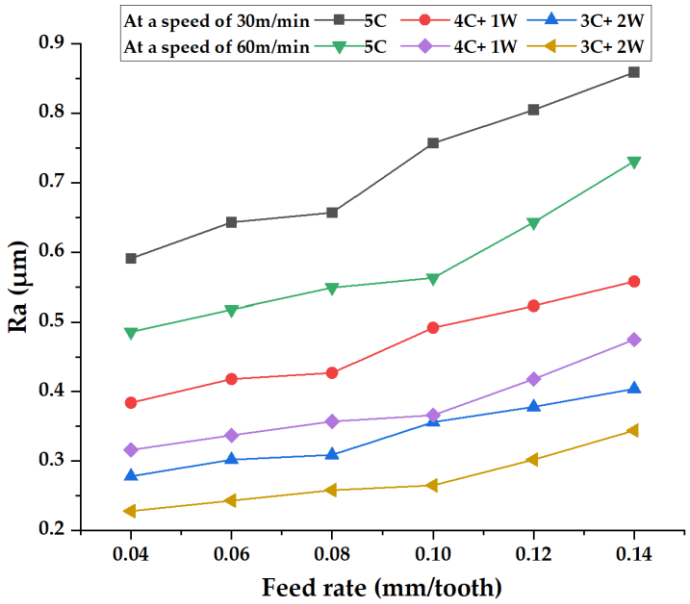

Figure 8. Correlation among feed rate and Ra for three machining scenarios at different cutting speeds.

In Figure 9, Rt and Rz are compared across different machining scenarios at a fixed cutting speed of 30 m/min. The results show that the third scenario, which employs two wiper inserts, achieves the lowest Rt and Rz values. This outcome emphasizes the effectiveness of using multiple wiper inserts to reduce the peaks of the roughness profile, thereby enhancing the surface finish.

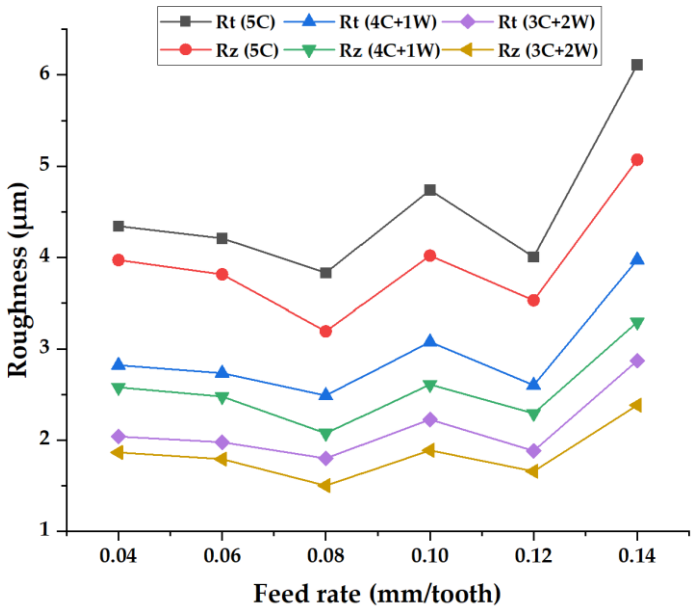

Figure 9. Correlation among feed rate and Rt and Rz for three machining scenarios.

The analysis reveals that a feed rate of 0.12 mm/tooth acts as a critical threshold for surface roughness. Below this feed rate, the values of Rt and Rz remain relatively stable and low, suggesting that the surface quality is less sensitive to variations in feed rate within this range. However, beyond this threshold, both Rt and Rz exhibit a significant increase, indicating a marked deterioration in surface quality as the feed rate rises. This observation highlights the importance of maintaining the feed rate below a certain level to preserve

the integrity of the surface finish during machining, particularly when striving for optimal surface quality in precision manufacturing.

4.2. Effect of Process Parameters on Power Consumption and MRR

MRR is calculated using Equations (2)–(4), and their values are listed in Table 4. It is observed that MRR has a direct proportionality with both cutting speed and feed rate, as shown in Figure 10. This relationship is attributed to their combined effect on enhancing chip removal efficiency, thereby increasing MRR. While high productivity is essential for economic benefits, escalating the feed rate imposes higher demands on power to counteract the increased generated cutting forces and temperature of the process zone, as depicted in Figure 11. Moreover, while higher cutting speeds can improve surface quality, they also lead to a substantial 40% increase in power consumption when the feed rate reaches 0.14 mm/teeth, a trend also shown in Figure 11. Additionally, the use of wiper inserts, which feature a larger contact area with the workpiece, further elevates power consumption. Specifically, each wiper insert added to the milling cutter raises the power consumption by an additional 5%. Given these dynamics, it is crucial to fine-tune the process parameters to establish an equilibrium between power usage, productivity, and attaining the requisite surface quality standards for machined products. Optimizing these parameters ensures that manufacturing processes remain economically viable while adhering to desired performance criteria.

$$MRR = w \times d \times f_m \quad (2)$$

$$f_m = N \times n_t \times f_t \quad (3)$$

$$N = 1000 \times V/(\Pi \times D) \quad (4)$$

where w is the width of cut (mm), d is the depth of cut (mm), f_m is the feed rate (mm/min), and N is the spindle speed (rpm). n_t is the number of teeth on the cutter, ft is the chip load in mm/tooth, V is the surface speed (meter/min), $\Pi = 3.14$, and D is the cutter diameter.

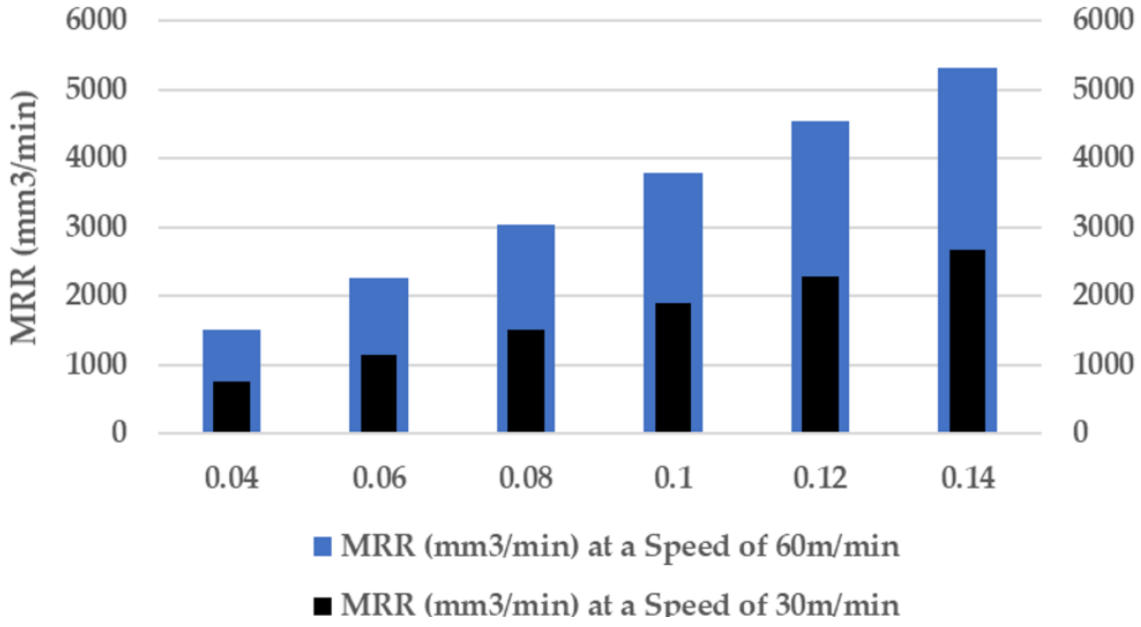

Figure 10. Correlation between feed rate and MRR at different cutting speeds.

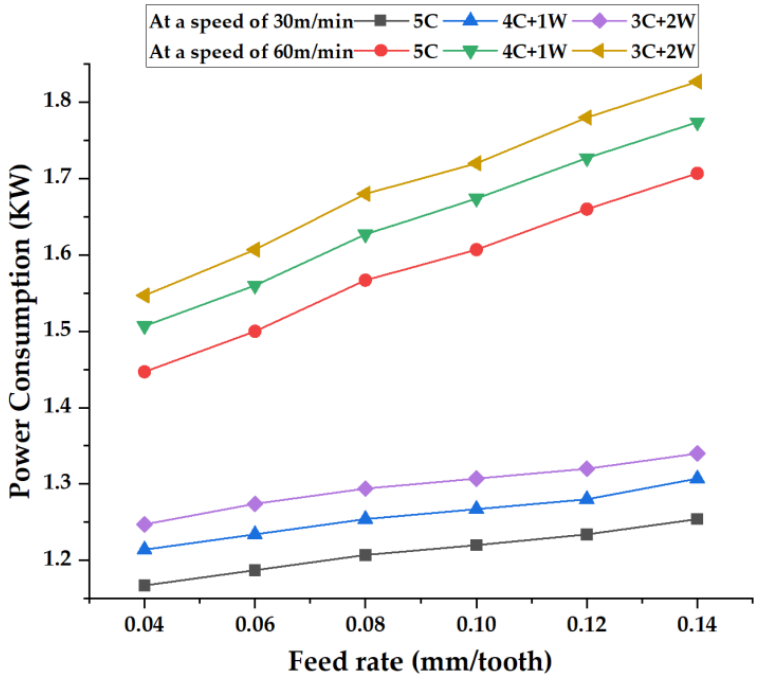

Figure 11. Correlation among feed rate and PC for the three machining scenarios at different cutting speeds.

5. Grey Relational Analysis

Machining is inherently a complex, multivariate process characterized by significant uncertainty and often unclear interrelationships among various process variables. Grey relational analysis (GRA) offers a robust methodology to simplify multi-objective optimization problems by condensing them into a singular optimization metric known as the grey relational grade (GRG). This grade serves as a composite indicator reflecting multiple performance characteristics [38]. GRA is particularly adept at addressing the challenges posed by uncertainty, multiple input variables, and discrete data sets in machining processes [39]. In this context, the framework of grey systems theory conceptualizes the unknown or uncertain information as 'black', well-defined information as 'white', and information that is partially known or uncertain as 'grey'. The grey system thus occupies a conceptual space that bridges the fully known (white) and the completely unknown (black) [40]. The determination of the GRG involves several key steps, outlined as follows:

5.1. Data Pre-Processing

The numerical data representing the performance characteristics (Ra, Rt, Rz, power consumption (PC), and material removal rate (MRR)) are initially normalized within a zero to one range, a process termed 'grey relational generation', as illustrated in Table 5. This normalization facilitates a consistent comparison across different scales and magnitudes of the data. For the analysis of these normalized values, the methodology is tailored based on the desired direction of optimization for each parameter. There are three principal approaches to interpret the normalized data: 'higher-the-better', 'smaller-the-better', and 'nominal-the-better' [41]. Each approach is selected based on the specific optimization goals associated with the different performance characteristics being evaluated.

Table 5. Normalized responses and deviation sequence.

Test No.	Normalization					Deviation Sequence				
	Ra (μm)	Rt (μm)	Rz (μm)	PC (KW)	MRR (mm^3/min)	Ra (μm)	Rt (μm)	Rz (μm)	PC (KW)	MRR (mm^3/min)
1	0.4247	0.3759	0.2881	1.0000	0.0000	0.5753	0.6241	0.7119	0.0000	1.0000
2	0.3423	0.4043	0.3291	0.9697	0.0836	0.6577	0.5957	0.6709	0.0303	0.9164
3	0.3201	0.4845	0.4911	0.9394	0.1673	0.6799	0.5155	0.5089	0.0606	0.8327
4	0.1616	0.2921	0.2755	0.9197	0.2509	0.8384	0.7079	0.7245	0.0803	0.7491
5	0.0856	0.4474	0.4037	0.8985	0.3346	0.9144	0.5526	0.5963	0.1015	0.6654
6	0.0000	0.0000	0.0000	0.8682	0.4182	1.0000	1.0000	1.0000	0.1318	0.5818
7	0.5911	0.6614	0.6319	0.5758	0.1662	0.4089	0.3386	0.3681	0.4242	0.8338
8	0.5404	0.4641	0.4335	0.4955	0.3330	0.4596	0.5359	0.5665	0.5045	0.6670
9	0.4913	0.6653	0.6120	0.3939	0.4997	0.5087	0.3347	0.3880	0.6061	0.5003
10	0.4691	0.1402	0.3516	0.3333	0.6665	0.5309	0.8598	0.6484	0.6667	0.3335
11	0.3423	0.3235	0.3229	0.2530	0.8331	0.6577	0.6765	0.6771	0.7470	0.1669
12	0.2029	0.2295	0.2329	0.1818	1.0000	0.7971	0.7705	0.7671	0.8182	0.0000
13	0.7528	0.6981	0.6515	0.9288	0.0000	0.2472	0.3019	0.3485	0.0712	1.0000
14	0.6989	0.7166	0.6782	0.8985	0.0836	0.3011	0.2834	0.3218	0.1015	0.9164
15	0.6846	0.7688	0.7836	0.8682	0.1673	0.3154	0.2312	0.2164	0.1318	0.8327
16	0.5816	0.6438	0.6434	0.8485	0.2509	0.4184	0.3562	0.3566	0.1515	0.7491
17	0.5325	0.7446	0.7266	0.8288	0.3346	0.4675	0.2554	0.2734	0.1712	0.6654
18	0.4770	0.4540	0.4642	0.7879	0.4182	0.5230	0.5460	0.5358	0.2121	0.5818
19	0.8605	0.8838	0.8749	0.4848	0.1662	0.1395	0.1162	0.1251	0.5152	0.8338
20	0.8273	0.7556	0.7462	0.4045	0.3330	0.1727	0.2444	0.2538	0.5955	0.6670
21	0.7956	0.8863	0.8621	0.3030	0.4997	0.2044	0.1137	0.1379	0.6970	0.5003
22	0.7813	0.5450	0.6928	0.2318	0.6665	0.2187	0.4550	0.3072	0.7682	0.3335
23	0.6989	0.6642	0.6743	0.1515	0.8331	0.3011	0.3358	0.3257	0.8485	0.1669
24	0.6086	0.6031	0.6156	0.0803	1.0000	0.3914	0.3969	0.3844	0.9197	0.0000
25	0.9208	0.8640	0.8386	0.8788	0.0000	0.0792	0.1360	0.1614	0.1212	1.0000
26	0.8827	0.8774	0.8577	0.8379	0.0836	0.1173	0.1226	0.1423	0.1621	0.9164
27	0.8716	0.9149	0.9338	0.8076	0.1673	0.1284	0.0851	0.0662	0.1924	0.8327
28	0.7971	0.8246	0.8325	0.7879	0.2509	0.2029	0.1754	0.1675	0.2121	0.7491
29	0.7623	0.8975	0.8927	0.7682	0.3346	0.2377	0.1025	0.1073	0.2318	0.6654
30	0.7211	0.6873	0.7030	0.7379	0.4182	0.2789	0.3127	0.2970	0.2621	0.5818
31	1.0000	0.9981	1.0000	0.4242	0.1662	0.0000	0.0019	0.0000	0.5758	0.8338
32	0.9762	0.9054	0.9069	0.3333	0.3330	0.0238	0.0946	0.0931	0.6667	0.6670
33	0.9525	1.0000	0.9906	0.2227	0.4997	0.0475	0.0000	0.0094	0.7773	0.5003
34	0.9414	0.7533	0.8684	0.1621	0.6665	0.0586	0.2467	0.1316	0.8379	0.3335
35	0.8827	0.8394	0.8548	0.0712	0.8331	0.1173	0.1606	0.1452	0.9288	0.1669
36	0.8162	0.7951	0.8124	0.0000	1.0000	0.1838	0.2049	0.1876	1.0000	0.0000

In this study, surface roughness (Ra, Rt, Rz) and power consumption (PC) are targeted for minimization and hence are categorized under the 'smaller-the-better' criterion. This means that lower values are preferred for these parameters, indicating better performance. Therefore, the normalization process for Ra, Rt, Rz, and PC adjusts the original data such that lower raw values translate to higher normalized values, aligning with the objective of minimizing these variables. The expression to calculate the normalized value for these 'smaller-the-better' characteristics will be outlined following this methodology, enabling a unified and objective comparison across all performance metrics, and can be expressed as:

$$x_{ij} = \frac{\max(y_{ij}) - y_{ij}}{\max(y_{ij}) - \min(y_{ij})} \quad (5)$$

While the material removal rate, which is a higher-the-better performance characteristic, can be expressed as:

$$x_{ij} = \frac{y_{ij} - \min(y_{ij})}{\max(y_{ij}) - \min(y_{ij})} \quad (6)$$

where y_{ij} represents the original numerical data of each response

5.2. Grey Relational Coefficient and Grey Relational Grade

In a subsequent grey relational generation, a grey relational coefficient is determined to represent the correlation between the ideal and actual normalized experimental results. The grey relational coefficient $\xi_i(k)$ for the kth performance characteristics in the ith experiment set can be described in Equation (7) [42].

$$\xi_i(k) = \frac{\Delta_{min} + \xi\, \Delta_{max}}{\Delta_{0i}(k) + \xi\, \Delta_{max}} \tag{7}$$

where Δ_{0i} denotes the deviation sequence, Equation (5), which means that the absolute value of the difference between $X_i^0(k)$ and $X_i^*(k)$.

$$\Delta_{0i} = ||X_0^*(k) - X_i^*(k)|| \tag{8}$$

$$\Delta_{min} = \min_{\forall j \in i} \min_{\forall k} \left|\left|X_0^*(k) - X_j^*(k)\right|\right| \tag{9}$$

$$\Delta_{max} = \max_{\forall j \in i} \max_{\forall k} \left|\left|X_0^*(k) - X_j^*(k)\right|\right| \tag{10}$$

where $X_0^*(k)$ donates reference sequence. ξ is the distinguishing coefficient that takes a value between zero and unity depending on the system requirement. In general, ξ = 0.5, and the deviation sequence is listed in Table 5, while the grey relational coefficient is listed in Table 6. Next, calculate the grey relational grade γ_i by taking the average value of the grey relational coefficients. The grey relational grade can be expressed as:

$$\gamma_i = \frac{1}{n} \sum_{k=1}^{n} \xi_i(k) \tag{11}$$

Table 6. Grey relational coefficient, grade, and grade ranking.

Test No.	Grey Relational Coefficient					Grade	Rank
	Ra (μm)	Rt (μm)	Rz (μm)	PC (KW)	MRR (mm^3/min)		
1	0.4650	0.4448	0.4126	1.0000	0.3333	0.5311	25
2	0.4319	0.4563	0.4270	0.9429	0.3530	0.5222	28
3	0.4238	0.4924	0.4956	0.8919	0.3752	0.5358	24
4	0.3736	0.4139	0.4083	0.8616	0.4003	0.4916	32
5	0.3535	0.4750	0.4561	0.8312	0.4290	0.5090	31
6	0.3333	0.3333	0.3333	0.7914	0.4622	0.4507	36
7	0.5501	0.5963	0.5759	0.5410	0.3749	0.5276	26
8	0.5211	0.4827	0.4688	0.4977	0.4285	0.4798	34
9	0.4957	0.5990	0.5631	0.4521	0.4998	0.5219	29
10	0.4850	0.3677	0.4354	0.4286	0.5999	0.4633	35
11	0.4319	0.4250	0.4248	0.4010	0.7498	0.4865	33
12	0.3855	0.3936	0.3946	0.3793	1.0000	0.5106	30
13	0.6691	0.6235	0.5893	0.8753	0.3333	0.6181	15
14	0.6241	0.6382	0.6084	0.8312	0.3530	0.6110	16
15	0.6132	0.6838	0.6980	0.7914	0.3752	0.6323	14
16	0.5444	0.5840	0.5837	0.7674	0.4003	0.5760	22
17	0.5168	0.6619	0.6465	0.7449	0.4290	0.5998	19
18	0.4888	0.4780	0.4827	0.7021	0.4622	0.5228	27
19	0.7819	0.8114	0.7999	0.4925	0.3749	0.6521	12

Table 6. *Cont.*

Test No.	Grey Relational Coefficient					Grade	Rank
	Ra (μm)	Rt (μm)	Rz (μm)	PC (KW)	MRR (mm^3/min)		
20	0.7432	0.6717	0.6633	0.4564	0.4285	0.5926	20
21	0.7098	0.8147	0.7838	0.4177	0.4998	0.6452	13
22	0.6957	0.5235	0.6194	0.3943	0.5999	0.5666	23
23	0.6241	0.5982	0.6055	0.3708	0.7498	0.5897	21
24	0.5609	0.5575	0.5654	0.3522	1.0000	0.6072	17
25	0.8632	0.7862	0.7559	0.8049	0.3333	0.7087	4
26	0.8100	0.8031	0.7784	0.7551	0.3530	0.6999	6
27	0.7957	0.8546	0.8831	0.7221	0.3752	0.7261	3
28	0.7114	0.7403	0.7491	0.7021	0.4003	0.6606	11
29	0.6778	0.8299	0.8234	0.6832	0.4290	0.6887	8
30	0.6419	0.6152	0.6274	0.6561	0.4622	0.6006	18
31	1.0000	0.9962	1.0000	0.4648	0.3749	0.7672	1
32	0.9546	0.8409	0.8430	0.4286	0.4285	0.6991	7
33	0.9132	1.0000	0.9815	0.3915	0.4998	0.7572	2
34	0.8950	0.6696	0.7916	0.3737	0.5999	0.6660	10
35	0.8100	0.7569	0.7749	0.3499	0.7498	0.6883	9
36	0.7312	0.7093	0.7272	0.3333	1.0000	0.7002	5

The grey relational grade, as presented in Table 6, is subsequently ranked to determine the hierarchy of the highest GRA values. This ranking process unveils that experiment number 31 represents the optimal combination of process parameters. This particular setup successfully minimizes the surface roughness parameters (Ra, Rt, Rz) and power consumption (Pc) while maximizing the material removal rate (MRR). The optimal parameter combination identified involves operating at a cutting speed of 60 m/min, a feed rate of 0.04 mm/tooth, and incorporating two wiper inserts in the milling cutter, aligning with the third scenario. This finding demonstrates the effectiveness of the selected parameters in achieving a balance between high productivity and optimal surface finish while maintaining efficient power usage.

6. Conclusions

The current study explored the impact of utilizing various numbers of wiper inserts on improving surface quality and productivity during the face-milling of maraging steel 350. The key findings from this investigation can be summarized as follows:

- Surface topography predictions were made for both wiper and standard inserts using the maximum height method. These predictions were then experimentally validated across three different machining setups. It was observed that employing two wiper inserts (as in the third scenario) significantly smoothens the roughness profile. This improvement is attributed to the increased contact area between the tool and the workpiece compared to other scenarios.
- Although the feed rate is inverse to the arithmetic average roughness (Ra), using a wiper insert mitigates the increase in Ra observed at higher feed rates.
- An increase in cutting speed results in a 40% rise in power consumption, primarily due to augmented friction between the cutting tool and the workpiece. Furthermore, each additional wiper insert contributes to a 5% increase in power consumption due to the larger contact area between the cutting tool and the workpiece, which increases the cutting forces.
- Incorporating more wiper inserts leads to better surface quality when machining maraging steel 350. However, it is important to note that wiper inserts are more expensive and consume more power than standard inserts. Thus, finding the optimal balance of wiper insert number and process parameters is crucial to meet industrial machining standards cost-effectively.

Through grey relational analysis optimization, the study identified an optimal combination of process parameters that maximizes surface quality and material removal rate (MRR) while minimizing power consumption. Specifically, a cutting speed of 60 m/min, a feed rate of 0.04 mm/tooth, and the use of two wiper inserts (the third scenario) were found to be the best settings. This optimal setup achieved a Ra of 0.228 µm, a power consumption (PC) of 1.547 kW, and an MRR of 1515 mm^3/min.

The research highlights the importance of precision in setting machining parameters to optimize the benefits of using wiper inserts. The specific settings that yielded the best results in this study serve as a valuable reference for similar machining tasks. However, the findings also suggest areas for further research, such as investigating the long-term wear of wiper inserts compared to standard inserts under similar machining conditions or exploring the impact of using wiper inserts on the lifespan of the milling machine due to the increased power consumption. Additionally, the study might prompt further investigation into the scalability of these results to other types of materials or different milling operations, expanding the applicability of the findings. Finally, the environmental aspect could also be considered, where the increased energy consumption with wiper inserts might have implications for the carbon footprint of the machining process, an angle that could be explored in future studies.

Author Contributions: A.T.A., M.O.H. and A.E: investigation, conceptualization, methodology, data curation, validation, and visualization; M.O.H., K.F.A., S.P. and A.S.H.: investigation, formal analysis, writing, and project administration; M.O.H.: writing original draft; A.T.A. and A.E.: supervision, and review and editing; A.T.A.: funding acquisition. All authors have read and agreed to the published version of the manuscript.

Funding: King Saud University-Project number (RSPD2024R1064).

Institutional Review Board Statement: Not applicable.

Informed Consent Statement: Not applicable.

Data Availability Statement: The raw data supporting the conclusions of this article will be made available by the authors on request.

Acknowledgments: The authors extend their appreciation to King Saud University for funding this work through Researchers Supporting Project number (RSPD2024R1064), King Saud University, Riyadh, Saudi Arabia.

Conflicts of Interest: The authors declare that they have no known conflicts of interest.

References

1. Pardal, J.; Tavares, S.; Terra, V.; Da Silva, M.; Dos Santos, D. Modeling of precipitation hardening during the aging and overaging of 18Ni–Co–Mo–Ti maraging 300 steel. *J. Alloys Compd.* **2005**, *393*, 109–113. [CrossRef]
2. Abbas, A.T.; Helmy, M.O.; Al-Abduljabbar, A.A.; Soliman, M.S.; Hasan, A.S.; Elkaseer, A. Precision Face Milling of Maraging Steel 350: An Experimental Investigation and Optimization Using Different Machine Learning Techniques. *Machines* **2023**, *11*, 1001. [CrossRef]
3. Jägle, E.A.; Choi, P.-P.; Van Humbeeck, J.; Raabe, D. Precipitation and austenite reversion behavior of a maraging steel produced by selective laser melting. *J. Mater. Res.* **2014**, *29*, 2072–2079. [CrossRef]
4. Casalino, G.; Campanelli, S.; Contuzzi, N.; Ludovico, A. Experimental investigation and statistical optimisation of the selective laser melting process of a maraging steel. *Opt. Laser Technol.* **2015**, *65*, 151–158. [CrossRef]
5. Reji, R.M.; Mohan, M.; Harikrishnan, U.; Joseph, V.T.; Sreekumar, K.; Varghese, T. Simulation of metallurgical failure of a maraging steel tension rod. *Trans. Indian Inst. Met.* **2015**, *68*, 35–40. [CrossRef]
6. Nagarajan, S.; Muthuswamy, P. An experimental study of applying various cutting edges on wiper milling inserts in face milling aisi 1070 steel. *Int. J. Mech. Ind. Eng.* **2013**, *2*, 257–262.
7. Ezugwu, E.; Wang, Z.; Machado, A. The machinability of nickel-based alloys: A review. *J. Mater. Process. Technol.* **1999**, *86*, 1–16. [CrossRef]
8. Batish, A.; Bhattacharya, A.; Kaur, M.; Cheema, M.S. Hard turning: Parametric optimization using genetic algorithm for rough/finish machining and study of surface morphology. *J. Mech. Sci. Technol.* **2014**, *28*, 1629–1640. [CrossRef]
9. D'addona, D.; Raykar, S.J. Analysis of surface roughness in hard turning using wiper insert geometry. *Procedia CIRP* **2016**, *41*, 841–846. [CrossRef]

10. Krishnaiah, K.; Shahabudeen, P. *Applied Design of Experiments and Taguchi Methods*; PHI Learning Pvt. Ltd.: New Delhi, India, 2012.
11. Muthuswamy, P. A novel wiper insert design and an experimental investigation to compare its performance in face milling. *Adv. Mater. Process. Technol.* **2022**, *8*, 2070–2085. [CrossRef]
12. Chinchanikar, S.; Choudhury, S. Wear behaviors of single-layer and multi-layer coated carbide inserts in high speed machining of hardened AISI 4340 steel. *J. Mech. Sci. Technol.* **2013**, *27*, 1451–1459. [CrossRef]
13. Davoudinejad, A.; Noordin, M. Effect of cutting edge preparation on tool performance in hard-turning of DF-3 tool steel with ceramic tools. *J. Mech. Sci. Technol.* **2014**, *28*, 4727–4736. [CrossRef]
14. Dogra, M.; Sharma, V.S. Machinability and surface quality issues in finish turning of hardened steel with coated carbide and CBN tools. *Mater. Manuf. Process.* **2012**, *27*, 1110–1117. [CrossRef]
15. Bouchelaghem, H.; Yallese, M.; Mabrouki, T.; Amirat, A.; Rigal, J.F. Experimental investigation and performance analyses of CBN insert in hard turning of cold work tool steel (D3). *Mach. Sci. Technol.* **2010**, *14*, 471–501. [CrossRef]
16. Patel, V.D.; Gandhi, A.H. Analysis and modeling of surface roughness based on cutting parameters and tool nose radius in turning of AISI D2 steel using CBN tool. *Measurement* **2019**, *138*, 34–38. [CrossRef]
17. Hua, Y.; Liu, Z. Effects of cutting parameters and tool nose radius on surface roughness and work hardening during dry turning Inconel 718. *Int. J. Adv. Manuf. Technol.* **2018**, *96*, 2421–2430. [CrossRef]
18. Abbas, A.T.; Sharma, N.; Soliman, M.S.; El Rayes, M.M.; Sharma, R.C.; Elkaseer, A. Effect of Wiper Edge Geometry on Machining Performance While Turning AISI 1045 Steel in Dry Conditions Using the VIKOR-ML Approach. *Machines* **2023**, *11*, 719. [CrossRef]
19. Szablewski, P.; Legutko, S.; Mróz, A.; Garbiec, D.; Czajka, R.; Smak, K.; Krawczyk, B. Surface Topography Description after Turning Inconel 718 with a Conventional, Wiper and Special Insert Made by the SPS Technique. *Materials* **2023**, *16*, 949. [CrossRef] [PubMed]
20. Çetindağ, H.A.; Çiçek, A.; Uçak, N.; Aslantas, K. Performance of conventional and wiper CBN inserts under various cooling conditions in hard turning of AISI 52100 steel. *Mater. Test.* **2023**, *66*, 288–298. [CrossRef]
21. Tan, J.; Wang, J.; Hao, X.; Ai, X.; Guo, G.; Lu, L.; Yang, Z.; Li, L.; He, N. Research on coated wiper insert for milling of compacted graphite iron. *Int. J. Adv. Manuf. Technol.* **2024**, *132*, 1237–1249. [CrossRef]
22. Sandvik Coromant. Available online: https://www.sandvik.coromant.com/en-gb/knowledge/milling (accessed on 24 April 2024).
23. Correia, A.E.; Davim, J.P. Surface roughness measurement in turning carbon steel AISI 1045 using wiper inserts. *Measurement* **2011**, *44*, 1000–1005. [CrossRef]
24. Zhang, P.; Liu, Z.; Guo, Y. Machinability for dry turning of laser cladded parts with conventional vs. wiper insert. *J. Manuf. Process.* **2017**, *28*, 494–499. [CrossRef]
25. Davim, J.P.; Figueira, L. Comparative evaluation of conventional and wiper ceramic tools on cutting forces, surface roughness, and tool wear in hard turning AISI D2 steel. *Proc. Inst. Mech. Eng. Part B J. Eng. Manuf.* **2007**, *221*, 625–633. [CrossRef]
26. Elbah, M.; Yallese, M.A.; Aouici, H.; Mabrouki, T.; Rigal, J.-F. Comparative assessment of wiper and conventional ceramic tools on surface roughness in hard turning AISI 4140 steel. *Measurement* **2013**, *46*, 3041–3056. [CrossRef]
27. Amini, S.; Paktinat, H. Ceramic tools with ordinary and wiper inserts in near dry machining with high speed on super alloy Monel K500. *Mater. Manuf. Process.* **2014**, *29*, 579–584. [CrossRef]
28. Abbas, A.T.; El Rayes, M.M.; Luqman, M.; Naeim, N.; Hegab, H.; Elkaseer, A. On the Assessment of Surface Quality and Productivity Aspects in Precision Hard Turning of AISI 4340 Steel Alloy: Relative Performance of Wiper vs. Conventional Inserts. *Materials* **2020**, *13*, 2036. [CrossRef]
29. Grzesik, W.; Wanat, T. Surface finish generated in hard turning of quenched alloy steel parts using conventional and wiper ceramic inserts. *Int. J. Mach. Tools Manuf.* **2006**, *46*, 1988–1995. [CrossRef]
30. Guddat, J.; M'saoubi, R.; Alm, P.; Meyer, D. Hard turning of AISI 52100 using PCBN wiper geometry inserts and the resulting surface integrity. *Procedia Eng.* **2011**, *19*, 118–124. [CrossRef]
31. Klocke, F.; Kratz, H. Advanced tool edge geometry for high precision hard turning. *CIRP Ann.* **2005**, *54*, 47–50. [CrossRef]
32. Abrão, A.M.; Aspinwall, D.K. The surface integrity of turned and ground hardened bearing steel. *Wear* **1996**, *196*, 279–284. [CrossRef]
33. Poulachon, G.; Bandyopadhyay, B.; Jawahir, I.; Pheulpin, S.; Seguin, E. Wear behavior of CBN tools while turning various hardened steels. *Wear* **2004**, *256*, 302–310. [CrossRef]
34. König, W.; Berktold, A.; Koch, K.-F. Turning versus grinding–a comparison of surface integrity aspects and attainable accuracies. *CIRP Ann.* **1993**, *42*, 39–43. [CrossRef]
35. Noordin, M.; Kurniawan, D.; Sharif, S. Hard turning of stainless steel using wiper coated carbide tool. *Int. J. Precis. Technol.* **2007**, *1*, 75–84. [CrossRef]
36. Özel, T.; Karpat, Y.; Figueira, L.; Davim, J.P. Modelling of surface finish and tool flank wear in turning of AISI D2 steel with ceramic wiper inserts. *J. Mater. Process. Technol.* **2007**, *189*, 192–198. [CrossRef]
37. Chen, W.; Lu, L.; Xie, W.; Huo, D.; Yang, K. A new surface topography-based method to quantify axial error of high speed milling cutters. *J. Manuf. Sci. Eng.* **2018**, *140*, 111014. [CrossRef]
38. Julong, D. Introduction to grey system theory. *J. Grey Syst.* **1989**, *1*, 1–24.

39. Kao, P.; Hocheng, H. Optimization of electrochemical polishing of stainless steel by grey relational analysis. *J. Mater. Process. Technol.* **2003**, *140*, 255–259. [CrossRef]
40. Helmy, M.O.; Fath El-Bab, A.R.; El-Hofy, H.A. Fabrication and characterization of polymethyl methacrylate microchannel using dry and underwater CO2 laser. *Proc. Inst. Mech. Eng. Part N J. Nanomater. Nanoeng. Nanosyst.* **2018**, *232*, 23–30. [CrossRef]
41. Palanikumar, K.; Latha, B.; Senthilkumar, V.; Davim, J.P. Analysis on drilling of glass fiber–reinforced polymer (GFRP) composites using grey relational analysis. *Mater. Manuf. Process.* **2012**, *27*, 297–305. [CrossRef]
42. Tosun, N. Determination of optimum parameters for multi-performance characteristics in drilling by using grey relational analysis. *Int. J. Adv. Manuf. Technol.* **2006**, *28*, 450–455. [CrossRef]